Interdependence between Structural Engineering and Construction Management
Edited by Ozevin, D., Ataei, H., Modares, M., Gurgun, A., Yazdani, S., and Singh, A.

ISBN: 978-0-9960437-6-2

DETERIORATION OF CONCRETE SULFUR STORAGE TANK UNDER ACIDIC VAPOR ATTACK

HASSAN A. KHALIFAH[1], MUHAMMAD K. RAHMAN[2], OMAR M. HAMDAN[4], MOHAMMED ABU HAID[4], MOHAMMED IBRAHIM[2], and ALI H. GADHIB[3]

[1]*Dept of Consulting Services, Saudi Aramco, Dhahran, Saudi Arabia,*
[2]*Research Institute, King Fahd University of Petroleum and Minerals, Dhahran, Saudi Arabia,*
[3]*Dept of Civil Engineering, King Fahd University of Petroleum and Minerals, Dhahran, Saudi Arabia,*
[4]*UGP Inspection Unit, Saudi Aramco, Dhahran, Saudi Arabia*

Sulfur storage tanks are integral parts of refineries and gas plants. During the gas sweetening process, liquid sulfur is separated in the sulfur recovery units and is stored in underground reinforced concrete tanks in liquid phase by steam-generated temperatures of 315 °F. Roof of the sulfur pit is about 300 – 400 mm thick reinforced concrete structure with two layers of reinforcement. Inside the sulfur pit, the ceiling and walls are subjected to high temperatures and highly corrosive acidic vapors above liquid sulfur line which leads to severe deterioration of concrete and corrosion of reinforcement in the roof slab. This paper presents the NDT based investigations of the roof slab of the tank using the Ground Penetrating Radar (GPR) in a typical sulfur pit with 30 years in service. GPR survey is compared with ultrasonic pulse echo and half-cell potential measurements on the slab. Compressive strength and petrographic examination of selected concrete cores and SEM/EDS and XRD tests on powder samples, from inside the pit are presented.

Keywords: Corrosion, Delamination, Service life, Condition assessment, Ground penetrating radar (GPR), Ultrasonic, SEM/EDS, Petrography.

1 INTRODUCTION

Natural gas obtained from Saudi Arabian sour gas fields contains significant amount of sulfur in the form of hydrogen sulphide. As a part of the gas treatment process, it is sent to the sulfur recovery units (SRU) to recover Sulfur. Typical SRU consist of a thermal reaction furnace, waste heat boilers, and a series of catalytic reactors (converters) and condensers. The sulfur generated from the process is stored in below-grade reinforced concrete sulfur storage tank (sulfur pits). (GPSA 2004).

Sulfur pits reinforced concrete structures are subjected to aggressive environment involving exposure to sulfur, sulfuric acid, vapor and moisture and elevated operating temperature (150°C). The roof slab of the sulfur pit is the primary element, which suffers from major deterioration due to reinforcing steel corrosion. Corrosion of reinforcement and spalling of concrete on the underside of the slab have been observed, resulting in severe reduction in load carrying capacity (Kline 2004, Kline 2006, Dowling 1992, Schwabenlander *et al.* 2004).

The sulfur pit under assessment has been in service for the past 30 years. It is a reinforced concrete structure constructed below grade level, consisting of retaining wall on the periphery covered with a reinforced concrete roof slab. The overall length of the sulfur pit is about 206.5 feet (63 m) and the width of the sulfur pit is about 48 feet (14.7 m). The roof slab is a 15 inches flat plate slab supported on column (with capital) at the center and retaining walls at the edges. The clear height of the sulfur pit is 7.5 feet. Walls and columns are supported on a raft foundation about 18 inches thick. The main objective of the study was to assess the potential of Ground Penetrating Radar (GPR) and Ultrasonic Impact Echo (UIE) techniques for NDT of roof slab of the sulfur pit. In addition to these NDT laboratory testing conducted includes compressive strength, petrographic examination and microstructural characterization.

2 RESULTS AND FINDINGS

2.1 Visual Inspection and Delamination Survey

Visual inspection of the roof slab was carried out to record distresses such as delamination and spalling. All defects observed during the visual inspection were measured and transferred to the drawings, as illustrated in Figure 1. The visual survey also included photographic evidence of the distresses found in the structural components of the sulfur pit. The delamination survey on the top of the roof slab was conducted by hammer sounding.

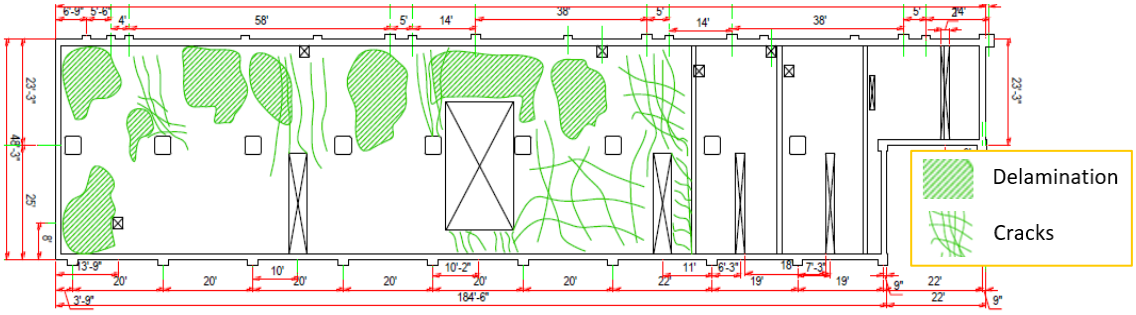

Figure 1. Cracking and delamination on the top side of the roof.

2.2 Ultrasonic Pulse Echo or Impact Echo

Ultrasonic pulse echo technique was used to detect flaws in the hardened concrete such as, delamination, cracks, honeycombing and voids. The ultrasonic pulse echo measurements were carried out on roof slab at a predetermined grid spacing of 2 feet in both horizontal and vertical directions. The technique is based on the propagation and reflection of shear waves using 50 kHz transducers. The average signal recorded by receiving transducers is presented as a 2D picture. The results of impact echo tests were plotted in a 2D format as shown in Figure 2. Irregularities in the concrete were identified based on the shear wave intensity as detailed in Table 1.

Table 1. Concrete quality based on shear wave speed.

Speed (m/s)	Concrete Quality
X<2000	Bad
2000>X>3000	Moderate
3000>X>4000	Very Good

The contour shown in figure 2 indicates very weak reflection of the shear waves around the openings. On the contrary, as we move from the openings the shear wave reflection was very strong. This shows that the concrete around the opening is weak or delaminated. The ultrasonic pulse echo results are in good agreement with the hammer survey carried out to determine delamination of concrete.

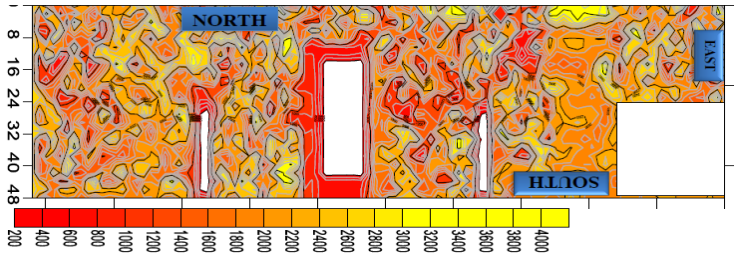

Figure 2. Ultrasonic pulse echo contours.

2.3 Corrosion Potential Measurements

Corrosion potential for detecting reinforcement corrosion and state of passivity of the reinforcing steel in concrete structures was based on (ASTM C876-09). Potentials were measured at a grid spacing of 2 x 2 feet, in longitudinal and transverse directions on the top of the roof slab. A reference electrode was placed on the concrete surface, which is connected via a high impedance Voltmeter (> 109 Ohms) to the reinforcement cage. Interpretation of the half-cell potential values, vis-a-vis the corrosion status, is shown in Table 2. Corrosion potential mapping for the roof slab is shown in Figure 3. It can be seen that the corrosion potential at several locations slab particularly around openings are higher than threshold value indicating that corrosion of steel is in progress in a large portion of the slab with some areas indicating high corrosion.

Table 2. Corrosion potential and their interpretation according to (ASTM C876-09).

Potential V (Vs $Cu/CuSO_4$)	Probability of Corrosion
<-0.35	> 95 %
-0.20 to -0.035	approx. 50 %
>-0.020	< 5 %

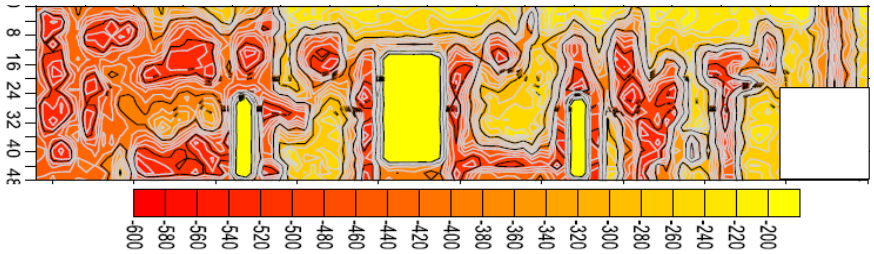

Figure 3. Corrosion potential mapping.

2.4 Ground Penetration Radar Survey

The GPR employed in this project is a high frequency 1600 MHz GPR (model GSSI), which can penetrate into the concrete to a depth of 0.5 meters. The overall thickness of the roof slab is 400

mm. GPR was also used to locate reinforcement in the concrete slab before extracting cores. All accessible rectangular areas were marked to conduct GPR survey. In each area GPR line scans were run two feet apart and analyzed to identify any anomalies in the substrate. These scans were taken using identical settings for the GPR equipment, data processing procedures, and scanning location to eliminate the impact of any parameter other than the concrete quality. Dielectric constant was assumed as 6.0, which corresponds to that of a dry concrete. Data was analyzed using the software RADAN by GSSI. The subsurface anomalies in the form of corrosion of steel reinforcement are shown in the Figure 4. It can be seen from this figure if the reinforcement is clean and not corroded there is a clear reflection of waves from the top reinforcement.

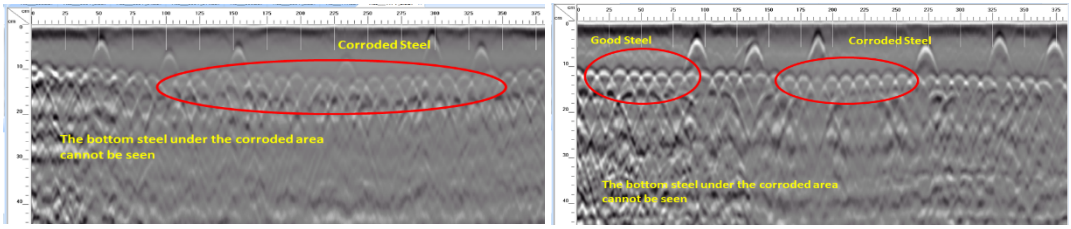

Figure 4. Reflection from top slab corroded reinforcing steel with GPR.

The estimated corrosion obtained from GPR analysis is shown in Figure 5. Severe to moderate corrosion of reinforcing steel is noted on the North side of the slab. Apart from this area, corrosion of steel is identified in a number of patches around the openings as well as in some cases away from it. The GPR results are in good agreement with the corrosion potential and impact echo tests.

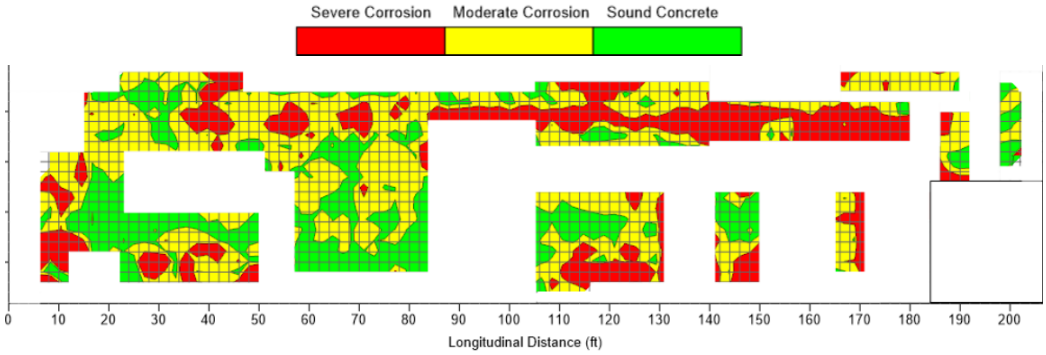

Figure 5. Estimated Corrosion based on GPR survey.

2.5 Compressive Strength of Concrete

Compressive strength of cored samples was determined according to (ASTM C39-12) and (ASTM C42-12). The compressive strengths of concrete cores obtained from the top slab at two locations were found to be 25.7 MPa and 16.9 MPa. According to the project specification, sulfate resistant cement was used with a minimum compressive strength of 24 MPa required after 28 days of curing.

2.6 Petrographic Analysis of Concrete

Petrographic examination according to (ASTM C856-11) "Standard Practice for Petrographic Examination of Hardened Concrete" was carried out on concrete specimens cored from the sulfur pit. Figure 6 shows a typical photomicrograph obtained from the concrete cores. The petrography of concrete core from the slab shows that the acidic sulfur vapors have affected the soffit of slab. The outer surface of the concrete core from the slab was worn and exhibited evidence of sulfur deposits. The concrete mix has nominal 19mm, crushed limestone/dolomite coarse aggregate and quartzitic sand fine aggregate, bound by a probable Portland-type cement matrix. The concrete is apparently well mixed, exhibiting good compaction. The excess voidage is about 0.5%. The petrography of concrete core from the slab shows that the acidic sulfur vapors have affected the soffit of slab. Top 10 mm seems to be heavily affected. Petrography shows weak, friable and cracked concrete in top 7 mm. There is a moderate level of sulfur penetration in the slab, up to a depth of 30 mm with voids and microcracks filled with sulfur. The maximum depth to which the sulfur has infiltrated into the slab is up to 60 mm. Alteration of the cement matrix and increased densification can be observed.

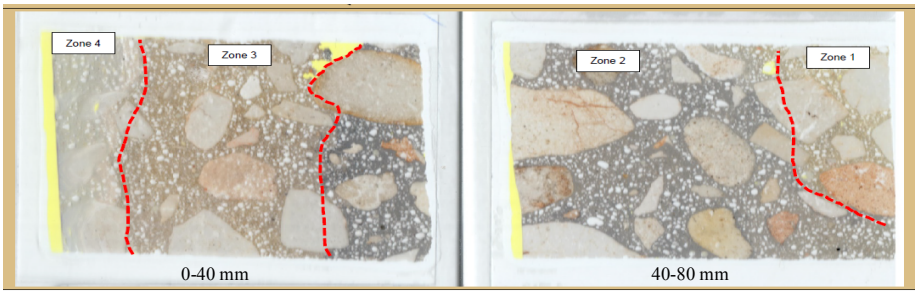

Figure 6. View of thin section showing zones of alteration within the concrete.

2.7 Microstructural Characterization

Scanning electron microscopy (SEM) and Energy dispersive x-ray spectroscopy (EDS) were used to determine the elemental composition of various phases in the specimens retrieved from underside of the roof slab at different depths. At each depth, elemental composition of different spots in the matrix was taken (Fig. 7). In the specimen extracted from 0 to 5 mm, 29.4% and 31.7% sulfur were noted at two different spots. Other elements such as Ca, Si, and Al were observed. Sulfur content was less at depth exceeding 5 mm from surface. High sulfur at the surface propagates the sulfate attack for the acids, resulting in formation of expansive material which causes cracking and delamination at the underside of roof slab.

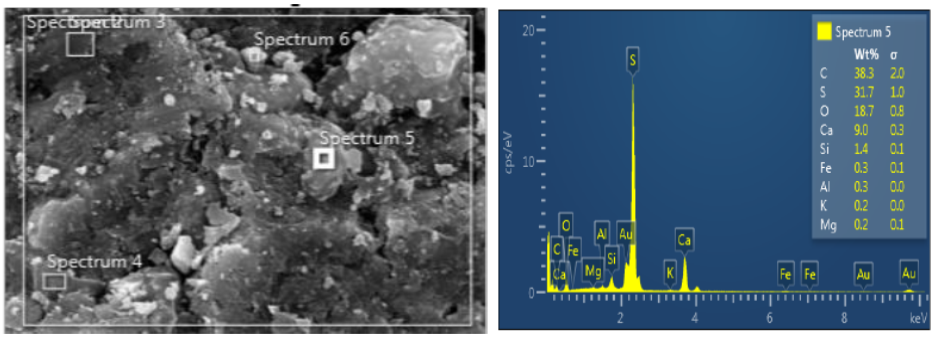

Figure 7. SEM and EDS of specimen extracted underside of roof from 0 to 5 mm depth.

2.8 X-Ray Diffraction (XRD)

Powder samples extracted from different structural components were analyzed. XRD for a powder sample collected from 0 to 5 mm from the surface (Figure 8) indicate presence of sulfur, anhydrite (calcium sulfate) and calcite peaks. Calcite, calcium silicate hydrate (CSH), anorthite, quartz and portlandite were also noted in the XRD patterns.

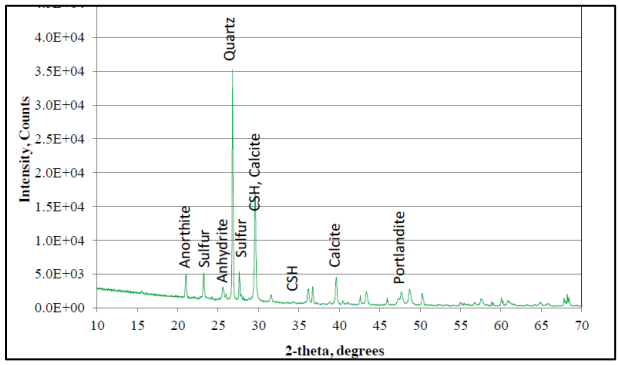

Figure 8. X-Ray diffraction of samples collected from underside of roof 0 to 5 mm from the surface.

3 CONCLUSIONS

GPR survey, impact echo and corrosion potential mapping suggested concrete delamination and to reinforcement corrosion on the top of the roof slab. GPR provided an excellent indication of corrosion severity at the top of the roof slab. However, the condition of the bottom reinforcement with the pit being operational cannot be diagnosed due to severe corrosion in top steel. Microstructural characterization and petrographic studies reveal the extent of deterioration.

References

ASTM C39, Standard Test Method for Compressive Strength of Cylindrical Concrete Specimens, ASTM International, West Conshohocken, PA, 8 Pages, 2012.

ASTM C42, Standard Test Method for Obtaining and Testing Drilled Cores and Sawed Beams of Concrete, ASTM International, West Conshohocken, PA, 7 Pages, 2012.

ASTM C856, Standard Practice for Petrographic Examination of Hardened Concrete, ASTM International, West Conshohocken, PA, 17 Pages, 2011.

ASTM C876. Standard Test Method for Corrosion Potentials of Uncoated Reinforcing Steel in Concrete, ASTM International, West Conshohocken, PA, 7 Pages, 2009.

Dowling, N. I., Corrosion of materials used in storage and handling of solid elemental sulphur, Alberta Sulphur Research, Ltd. Sulphur and Energy, 103-115, 1992.

GPSA, Engineering Data Book, FPS Version Volume I & II, Gas Processing Suppliers Association, 2004.

Kline, T., Sulfur Pit Assessment and Repair Strategies, Paper Presented at Brimstone Sulfur Symposium, Vail, Colorado, September 2004.

Kline, T., Repair of Subsurface Molten Sulfur Containment Structures, Paper Presented at Brimstone Sulfur Symposium, Banff, Alberta, CA, 2006.

Schwabenlander, R., and Kline, T., Sulfur-Recovery Operations Pose Formidable Challenge to Concrete Infrastructure, *World Refining,* 12(4), 30-31, May 2002.